CHARACTERIZATION OF HIGH TEMPERATURE SOLAR THERMAL SYSTEM USING NON-IMAGING FOCUSING HELIOSTAT

Loh Ying Zhe

A project report submitted in partial fulfilment of the requirements for the award of Master of Engineering (Electrical)

**Lee Kong Chian Faculty of Engineering and Science
Universiti Tunku Abdul Rahman**

April 2021

DECLARATION

I hereby declare that this project report is based on my original work except for citations and quotations which have been duly acknowledged. I also declare that it has not been previously and concurrently submitted for any other degree or award at UTAR or other institutions.

Signature : _____

Name : Loh Ying Zhe

ID No. : 2003486

Date : 18 April 2021

APPROVAL FOR SUBMISSION

I certify that this project report entitled **"CHARACTERIZATION OF HIGH TEMPERATURE SOLAR THERMAL SYSTEM USING NON-IMAGING FOCUSING HELIOSTAT"** was prepared by **LOH YING ZHE** has met the required standard for submission in partial fulfilment of the requirements for the award of Master of Electrical Engineering at Universiti Tunku Abdul Rahman.

Approved by,

Signature	:	K.K.Chong
Supervisor	:	Chong Kok Keong
Date	:	22/4/2021

Signature	:	
Co-Supervisor	:	
Date	:	

ACKNOWLEDGEMENTS

First and foremost, I would like to thank everyone who had contributed to the successful completion of this project. I would like to express my gratitude to my research supervisor, Dr. Chong Kok Keong for his providing the require materials and resources with invaluable advice, guidance and his enormous patience throughout the development of the research.

I would also like to thank to my parents, for understanding and supporting me both emotionally and financially. Without their support, this work may not be able to complete smoothly.

CHARACTERIZATION OF HIGH TEMPERATURE SOLAR THERMAL SYSTEM USING NON-IMAGING FOCUSING HELIOSTAT

ABSTRACT

The spinning-elevation method first suggested by Ries and Zaibel and in 2001, Chen et al. proposed a non-imaging focusing heliostat (NFIH) implementing the spinning-elevation method which capable of actively correcting the astigmatic aberration that exists in the traditional heliostat system. Since then, Chen et al. and Chong have collectively derived and developed the sun-tracking formula for the NIFH. In the thesis, formulas derived will be utilized to the simulation for the NIFH. The optimal simulated result within the shortest period are investigated and the factors that affect the efficiency of the NIFH such as circumsolar ratio (CSR) and slope error (SE) were studied and results show that with increased of CSR and SE, the spillage loss increases, heliostat efficiency dropped and causing a deviation to the flux distribution profile of the NIFH.

TABLE OF CONTENTS

LIST OF TABLES

LIST OF FIGURES

LIST OF SYMBOLS / ABBREVIATIONS

NIFH	Non-imaging focusing heliostat
SE	Slope error
CSR	Circumsolar ratio
n_{MR}	Mirror resolution
n_{SD}	Solar disc resolution

LIST OF APPENDICES

CHAPTER 1

INTRODUCTION

1.1   Research Background

Solar thermal systems generate electricity by collecting by concentrates sunlight to produce high temperature heat needed. The traditional solar furnaces include two or three optical configuration: flat heliostat for sun-tracking, secondary parabolic dish for focusing and additionally a tertiary non-imaging concentrator to achieve a higher concentration flux. The traditional heliostats however encounter astigmatic aberration which happens most of the time and is unavoidable due to the apparent motion of the sun during the day causing non-normal incident sunlight relative to the heliostat, leading to large variation of the incidence angle to the heliostat. The correction of the astigmatism are expensive with complicated control system with a total of 2 x m x n motors to focus each facet in group.

A better and improved heliostat is proposed by Chen et al. in 2001, a non-imaging focusing heliostat (NIFH) implementing manoeuvre of facets in the same tangential or sagittal group can be adjusted to certain angles during sun-tracking so that the astigmatic solar images are actively corrected.

The NFIH is designed with mirrors arranged to row and column. The centre column is maintained in the optical plane for the frame to be rotated. A master mirror is fixed at the centre with the purpose to target the solar image into the receiver. Surrounding the master mirror is the slave mirrors with two extra moving freedoms about their pivot point which angularly moved to reflect sun rays onto the same target as the master mirror into the receiver superposition the mirror images.

1.2   Problem Statement

The major challenge of the solar thermal system that incorporating the focusing heliostat is the astigmatism aberration that comes with the change of incident angle during sun-tracking. The astigmatism effect causes enlarged image area and reduces intensity which decreases the quality of a solar thermal system

The work is to perform simulation and optimization for the best performance with NIFH will be conducted. Characterization of the results is equally important to identify the variable that can be controlled for improvement of the research.

1.3   Research Objectives

The objectives of the research is to:
  i.   Investigate optimal simulation result and time through optimizing computational simulation parameters.
  ii. Study the effects of slope error and circumsolar ratio on NIFH.
  iii. Performing characteristics analysis of the NIFH.

CHAPTER 2

LITERATURE REVIEW

The mathematics of sun tracking which is the azimuth-elevation tracking formula has remained the same and been used for decades until the operating principle of the NIFH, the spinning-elevation, also called target-aligned tracking was first suggested by Ries and Zaibel in 1995 without segmented facet and focusing ability. The paper lacks the elevation tracking formula and prototype to show the functionality.

In 2001, Chen et al. first proposed a NIFH, a spinning- elevation tracking heliostat where all the small mirror facets can be adjusted to focus onto the same target as the master mirror, allowing astigmatic aberration to be corrected actively during sun-tracking. Since 2001, Chen et al. and Chong have collectively derived and developed the sun-tracking formula for the spinning-elevation method by proposing a novel focusing heliostat called non-imaging focusing heliostat (Chen et al., 2001, 2002,2003, 2004, 2005; Chong, 2002, 2010a,b; Chong et al., 2006, 2011). A new general form of solar-tracking formula of an arbitrary oriented heliostat toward the arbitrarily located target on the Earth which included all kinds of tracking methods are presented by Chen Y.T et. al. (2006).

Further to 2016, Lim et. al. proposed and demonstrated the Latitude-orientated configuration of non-imaging focusing heliostat with an array of 5x5 mirror facets prototype at Malaysia University of Science and Technology. The LO-NIFH configuration operates at a very narrow range of incident angle capable to produced wide range of solar concentration ratio around 50 to 500 suns are well suited to replace or to be integrated into the low conventional low- to medium temperature solar thermal energy gathering system.

For the solar furnace to achieve a higher solar concentration ratio to more than 20,000 suns, a conventional solar furnace system typically requires three-stage: a primary heliostat as a sun-tracker to reflect sunlight, a secondary parabolic concentrator to concentrate the sunlight moderately and a tertiary compound parabolic concentrator to further enhance the focused sunlight. Traditional solar furnace systems normally is

high in cost attributed to the large aperture size of the secondary parabolic concentrator, which is normally nearly the same size or even larger than that of the heliostat reflective area. 10-20 years ago a solar furnace using an uncorrected focusing heliostat and a parabola was tested in Germany or Israel or other countries with fairly poor results due to aberration of the tracing mirror. For instance, conventional solar furnaces built are the furnace of Arizona State College in the USA (Kevane, 1957), Solar Energy Research Institute (SERI) High-Flux Solar Furnace (Lewandowki, 1991), the furnace of the Government Institute for Industrial Research in Japan (Hisada et al., 1957), large solar furnace in Odeillo, France with 1000 kW (Trombe and Le Phat Vinh, 1973), large solar furnace of the Academy of Sciences of Uzbekistan with 1000 kW (Abdurakhamanov et al., 1998), the furnace of Paul Scherrer Institute (PSI), of 25–40 kW (Schubnell et al., 1991), the furnace of CIEMAT, in Plataforma Solar de Almerı´a, Spain with 45 kW (Fernandez-Reche et al. 2006), and the furnace of DLR, in Cologne, Germany, of 20 kW (Neumann and Groer, 1996).

To significantly reduce the size of a secondary concentrator of the solar furnace, NIFH has been proposed to perform both sun-tracking and sunlight focusing concurrently (Chen et al., 2001, 2002, 2003, 2004, 2006; Chong, 2010a, b; Chong et al., 2011a, b). In this context, the size of the secondary concentrator is very much dependent on how well the primary focusing can be performed by the NIFH heliostat. For cost-saving and reducing complication in the control system, a good approximation to full astigmatic aberration correction can be done with the application of a new spinning-elevation tracking method which preserves the vertical and horizontal directions of the heliostat frame to be always aligned with the tangential and sagittal planes respectively. With the new optical configuration, dynamic correction of astigmatism owing to the variation of incident angle can be greatly simplified by just moving element mirrors in a group manner so that those mirrors of the same row or column can share the same mechanical actuator. As a result, instead of employing 2 x m x n actuators, NIFH heliostat with dynamic geometry only requires $(m + n - 2)$ actuators to correct the first order of astigmatism. With the focusing task partially implemented by NIFH heliostat, the secondary concentrator can be significantly reduced by at least 25 times in the area, and hence ultra-high concentration can be achieved with only a two-stage system cost-effectively. In practice, Lim and Li (2009) have successfully demonstrated the new solar furnace using a 5 m × 5 m prototype NIFH and a much smaller spherical

concentrator with 70 cm in aperture size to achieve 25,000 suns in Ningxia province, P.R. China.

Other than solar power generation, the NIFH shows potential in another field such as food processing. The NIFH was tested to peel potato skin (Chen et al. 2005). To turn the Silicon into a photovoltaic material, the raw silicon has to be purified and the boron has to be removed. Additionally, using the new solar furnace, purification of metallurgical silicon into solar grade silicon is achieved and the boron is proposed to be extracted with the aid of the photo-chemical effect method (Chen et al., 2009, 2010). The method is a low-cost and simple process that has gained China's Top 10 Science and Technology Progressing Award of 2009 (Cressey, 2010).

With recent advances in the processing power of computers, computational simulation is widely applied in various complicated studies that could not be expressed in an analytical formula especially for design work of central receiver system, solar furnace, multiple stages of solar concentrators, etc. Simulation codes for traditional azimuth-elevation heliostat have been developed by several research groups which can be found in HELIOS (Vittitoe and Biggs, 1976), CIRCE (Ratzel et al., 1986), MIRVAL (Leary and Hankins, 1979), new code by Wei et al (2010), etc. The aforementioned codes are not suitable to model the dynamic geometry of NIFH heliostat due to its unique tracking method, and it also cannot be represented by any analytical model due to the complicated compound geometry. A comprehensive computational algorithm using the ray-tracing technique is required to analyse the optical characteristics of NIFH heliostat.

CHAPTER 3

METHODOLOGY

3.1 Research Procedures

The research is started with understanding the NIFH concepts and theory behind the heliostat's sun-tracking procedures and formula for its operation. Next, the analytical calculation is done for the simulator for optimal results. The NIFH heliostat simulator is developed with Microsoft Visual C++ by my project supervisor, Prof. Chong and the interface is as shown in Figure 2 are used for the simulation work while the pre-set settings for the simulation is as table 1, where Figure 3 is the device specification of the personal computer used for the simulation work. The simulation resolution, circumsolar ratio, and slope error will be discussed in the following section. After the simulation is done, an output file with values is created. The simulation is the most time-consuming procedure throughout the work, time taken for a higher resolution could take days to finish the simulation run. MATLAB code is next developed to read the output file and generate figures for visualization analysis.
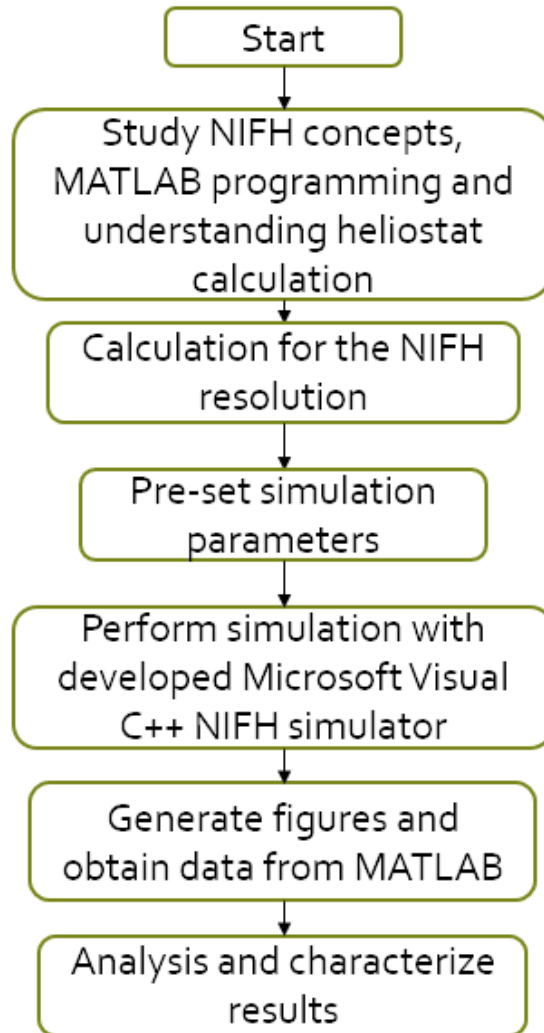
Figure 1 Methodology flowchart

Table 1 Pre-set setting for the simulation

Mirror Size, w	46	cm
Focal Size, fs	27	cm
Half angle, a	0.00465	0.00465
Target dist. L	2400	cm
Position, Lp	-6	
Target Size, Ts	25	cm
Row and Column	17	
Incident, Theta	14.05	degree
Canting, Op. Theta	36	degree
Number of pixel, ntr	201	
Image size, Is	25	cm
Mirror gap (cm)	0.5	cm
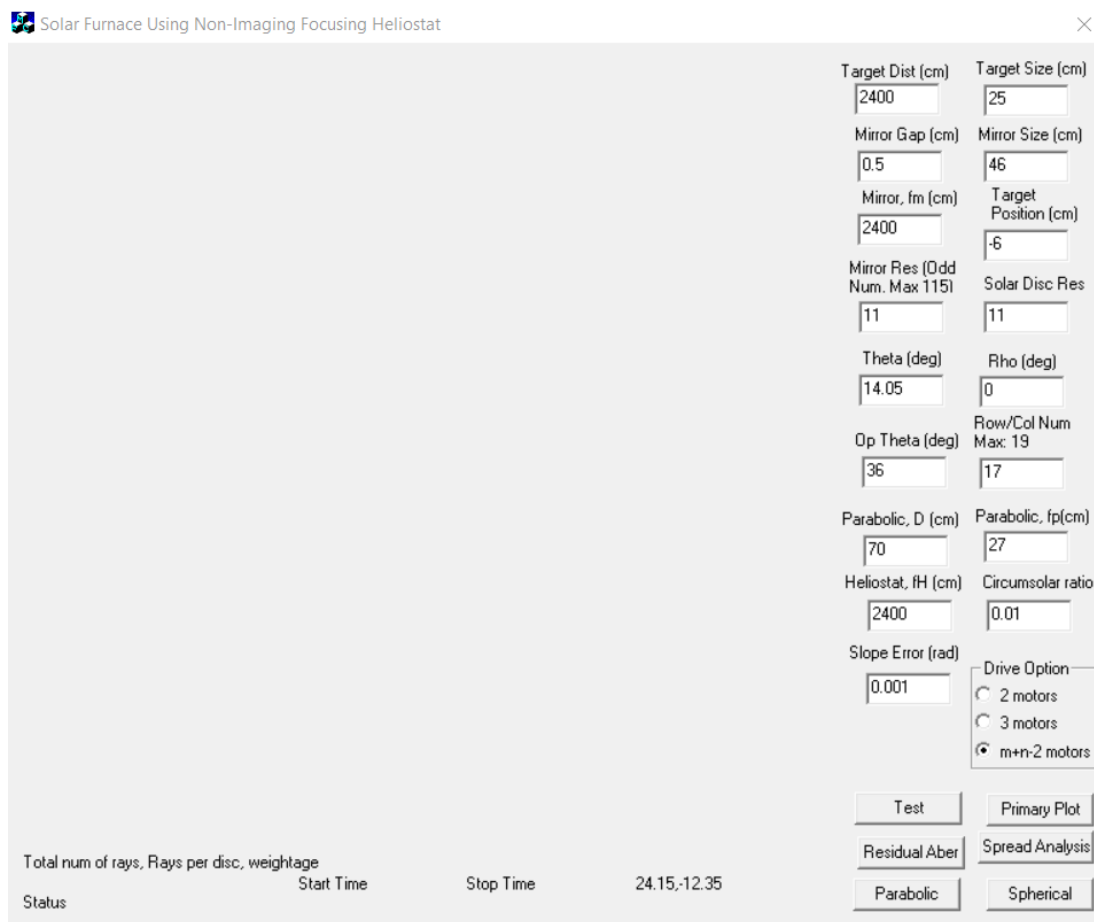
Figure 2 Solar furnace using NIFH simulator

Figure 3 Device specifications used for simulation work

3.2   Calculation for Optimal Mirror and Solar Disc Resolution

The resolution of the heliostat will be calculated before inputting for simulation. Table 1 are the pre-set settings for the simulation throughout the work and the input is used to calculate the mirror and solar disc resolution. The formula used to calculate the resolution is derived by Chong and Lim, 2013.

The target size, Ts is divided into the pixels which is 201 pixel in the study. The rMR is the resolution of mirror while rSD is the resolution for the solar disc. In the simulation, each element of mirror of heliostat with dimension of w is represented by number of reflective points, n_{MR} and the number of sub rays per aperture radius, n_{SD}.

Firstly, the correlation between rMR or rSD and r_{TR} can be calculated with following expression

$$rtr = \frac{ntr}{Ts} \tag{1}$$

$$rMR = k1 \; x \; rtr \; x \left(\frac{Is}{Hs}\right) \tag{2}$$

Where Heliostat size, Hs = (w x n) + mirror gap (n-1).

$$rSD = k2 \; x \; rtr \tag{3}$$

Table 2 Result for rMR and rSD

rTR	8.04	
rMR	0.25443	k1
rSD	8.04	k2

Then the n_{MR} and the n_{SD} can be obtain by

$$nMR = rMR \; x \; w \tag{4}$$

$$nSD = \frac{rSD \; x \; Dsd}{2} \tag{5}$$

The D_{SD} is the diameter of the receiver plane in cm and referring to Figure 1, the D_{SD} can be obtained from

$$Dsd = 2Ltan\,(a)\left[\,1 + \frac{(-Lp - fs)}{Ltan(\alpha)\tan(\,\alpha + \Psi)}\right.$$ (6)

Where α is the solar disc half angle of 4.65 mrad and the Ψ is can be calculated as

$$\Psi = \tan^{-1}(\frac{fs}{Ltan(\alpha)})$$ (7)
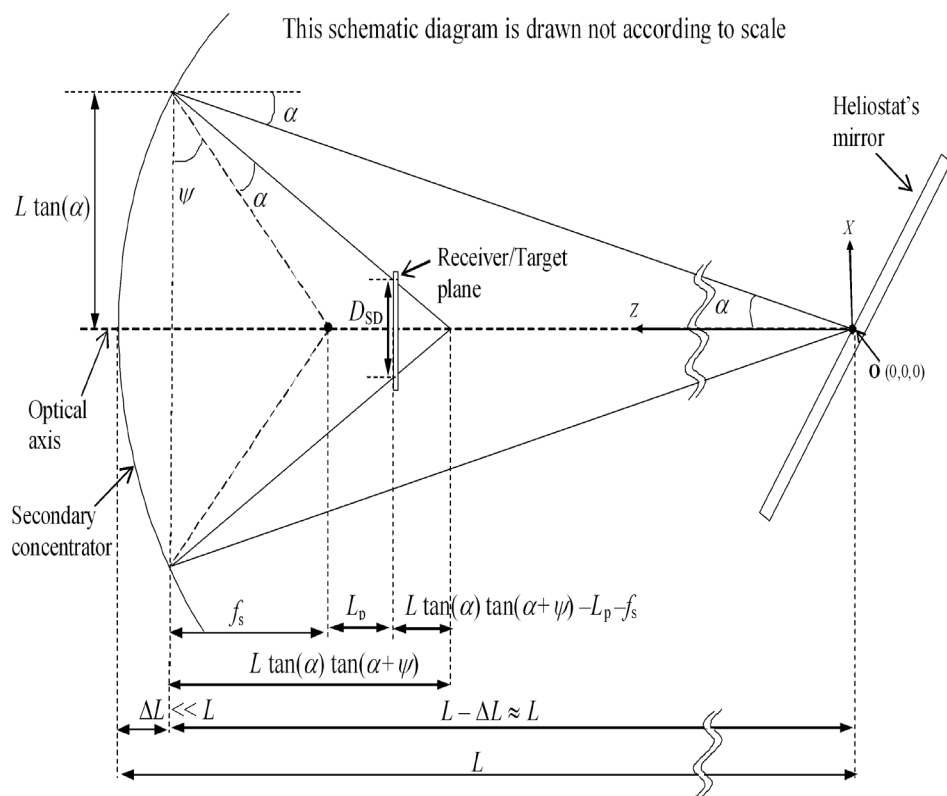
Figure 4 Schematic diagram to show how diameter of cone ray, D_{SD}, at the receiver plane is calculated (Chong and Lim, 2013)

The value calculated with the formula above is shown in table 3. Mirror resolution are increased by the n_{MR} with factor of k1 factor while solar disc resolution are increased by the n_{SD} with k2 factor as shown in table 4. Higher n_{SD} and n_{MR} is equivalent to higher heliostats resolution.

The table 4 calculated resolution is then rounded up to suit the input requirement of odd value for n_{MR} and even value for n_{SD}.

Table 3 value obtain from calculation

Ψ	1.178846	
Dsd	5.188265	
nmr	11.7038	k1
nsd	20.85683	k2

Table 4 Calculated resolution with increasing k1 and k2 factor.

		nmr	nsd	nmr	nsd	nmr	nsd	nmr	nsd
					k2				
		1	1	2	2	3	3	4	4
	1	11.7038	20.85683	11.7038	41.71365	11.7038	62.57048	11.7038	83.4273
	2	23.40759	20.85683	23.40759	41.71365	23.40759	62.57048	23.40759	83.4273
	3	35.11139	20.85683	35.11139	41.71365	35.11139	62.57048	35.11139	83.4273
	4	46.81519	20.85683	46.81519	41.71365	46.81519	62.57048	46.81519	83.4273
k1	5	58.51899	20.85683	58.51899	41.71365	58.51899	62.57048	58.51899	83.4273

Table 5 Resolutions adjusted for simulation

		k2							
		1	1	2	2	3	3	4	4
	1	11	20	11	40	11	60	11	80
	2	23	20	23	40	23	60	23	80
	3	35	20	35	40	35	60	35	80
	4	47	20	47	40	47	60	47	80
k1	5	59	20	59	40	59	60	59	80

3.3 Number of Ray

The number of rays/discs can be obtained from the simulator's interface as circled in Figure 5 while the row and column of 17 were used for all the simulations in the research. The number of rays to be traced in the simulation of each flux distribution profile can be calculated with the equation:

$$Number\ of\ ray = Nmr\ x\ Nsd\ x\ (Column\ x\ Row)x\ (\frac{ray}{disc}) \qquad \textbf{(8)}$$

Table 6 The resolution and corresponding ray/ disc and number of ray

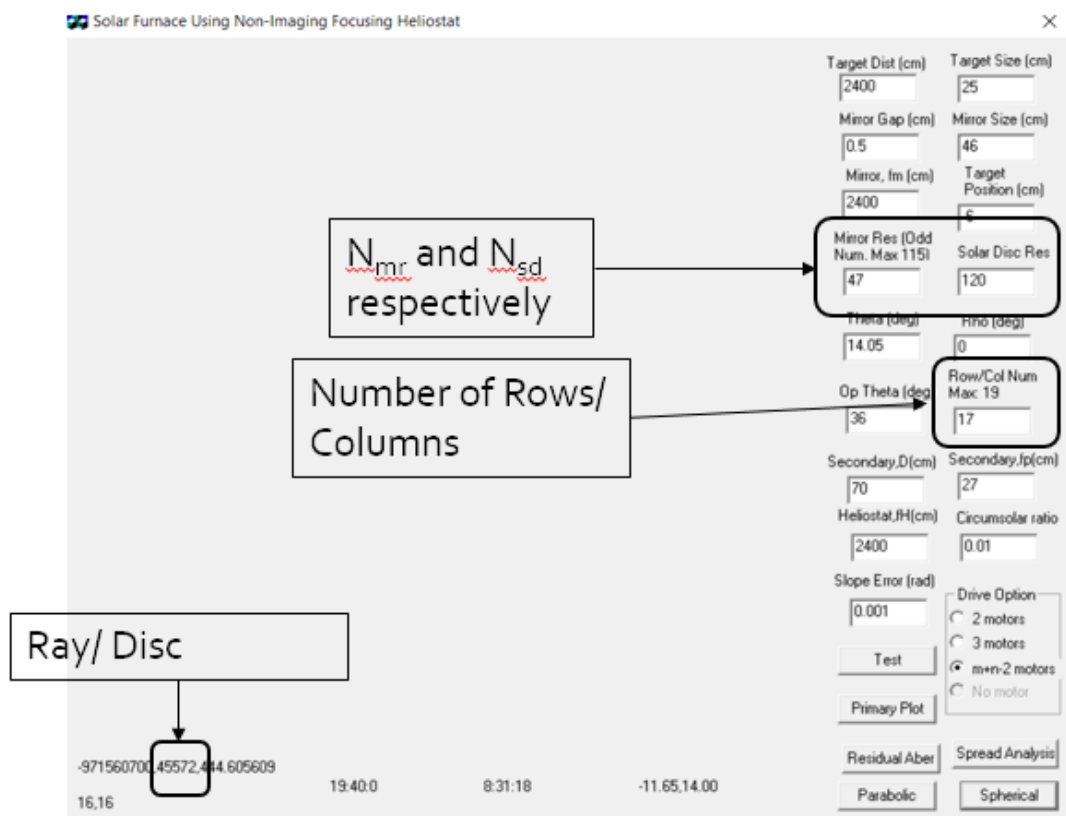| Nmr	Nsd	Ray/ Disc	Nray
47	20	1304	354244640
47	40	5140	2792664800
47	60	11476	9352710480
47	80	20332	22093564480
47	120	45572	74280537120

Figure 5 Number of ray/ disc location on the Solar Furnace NIFH simulator

3.4   Slope Error

Slope Error (SE) represents the degree of imperfections of the heliostat's mirror surfaces. These imperfections cause a local deviation of the surface slope, which in turn influences the direction of the reflection.

3.5   Circumsolar Ratio

Circumsolar radiation (CSR) can be described by the radiance emanating from the circumsolar region and the sun as a function of the angular distance from the center of the sun. CSR is varied according to the geographic location, climate, season, time of day, and the observing wavelength. The high value of CSR may cause overestimation of solar flux collected or altering the sunray width of the flux.

The solar concentration ratio (number of suns) of each pixel in the receiver plane is essentially a measure of how much solar irradiation that a pixel receives compared to the direct normal solar irradiation if there is a total count of N sub-rays hitting on a particular pixel and it is calculated as

$$CSR = \sum_{N-1}^{N} \frac{\left(\frac{w}{nMR}\right)^2}{\left(\frac{Ts}{nTR}\right)^2} \; x \cos\frac{\theta}{p} \tag{9}$$

3.6   Spillage

Spillage is the flux concentration reflected by the heliostat outside of the receiver domain. The spillage is used to study the efficiency of the heliostat. To calculate the spillage, the integration of the reflected flux of non-CSR SE output is compared with the integrated reflected flux affected by CSR and SE.
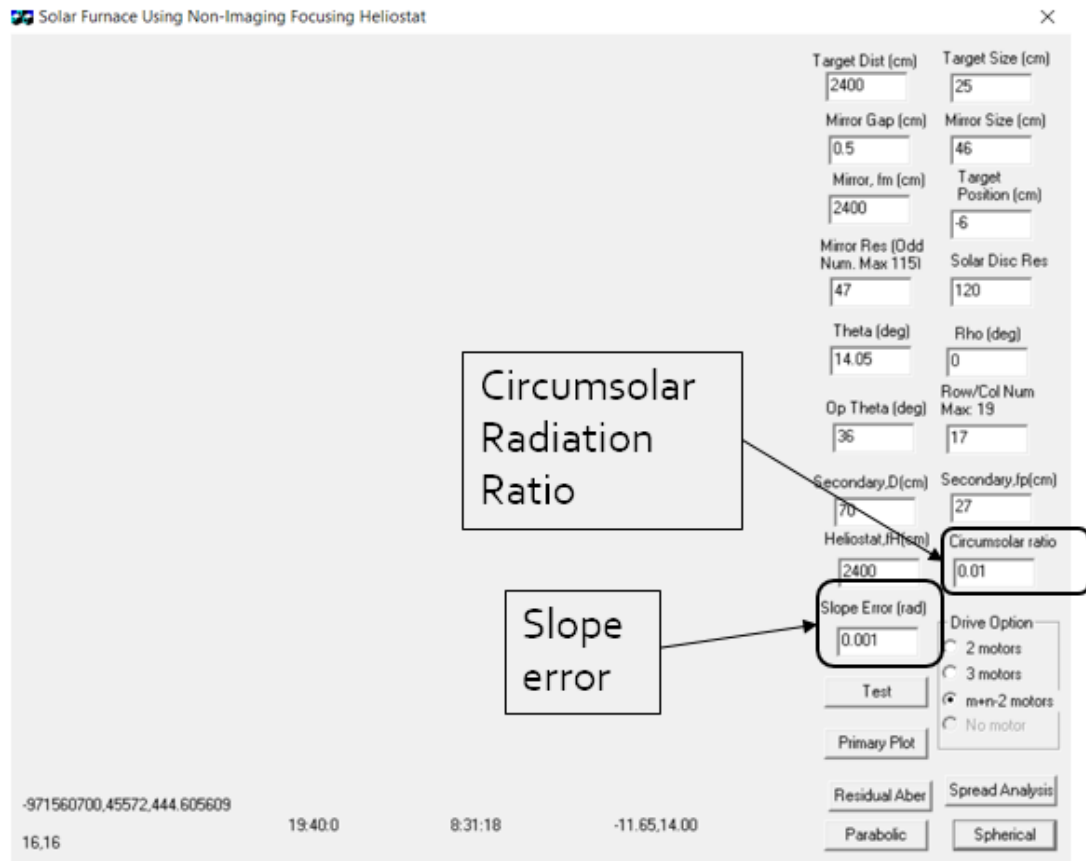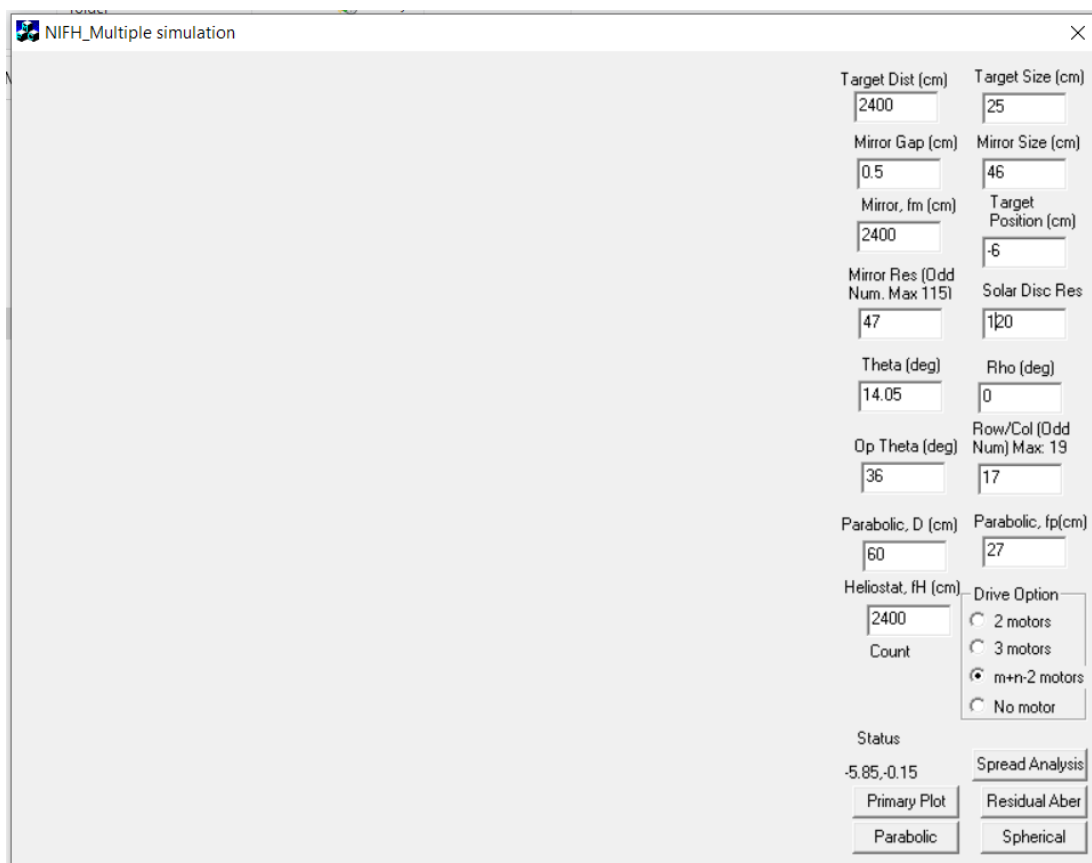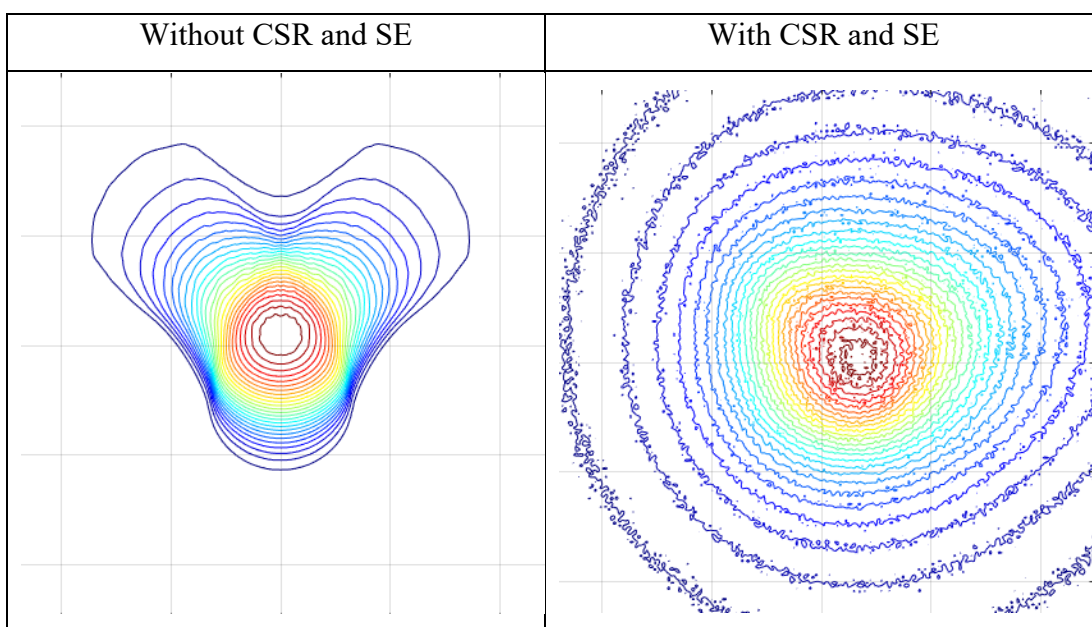
Figure 6 Location of resolution, CSR and SE input

Figure 7 The NIFH simulator version used to obtain non CSR SE output

Without CSR and SE	With CSR and SE

CHAPTER 4

RESULTS AND DISCUSSIONS

4.1   MATLAB Code Generation

First, three-line applied to the MATLAB code are 'clear', 'clc', and 'clf'. The 'clear' command removes the variable and frees up memory, 'clc' command clears the input and output from the window screen while the 'clf' resets all figure properties.

This code line locates, identify and open the file for reading and writing:

```
fid = fopen('C:\Directory Path\File Name.dat','r+');
[data,count]=fread(fid,[201,201],'double');
```

Error of the simulator resulting into abnormally high output of simulation data (1,1), the data(1,1) is set to 0:

```
data (1,1)= 0;
```

The data is stored to x and y, and the Target size used for simulation is input as follows:

```
data (1, 1) = 0;
x=1:201;
y=1:201;
global TargetSize %unit in cm
TargetSize=25;
```

The *'meshgrid'* function then transform the domain specified by x and y into arrays X and Y.

```
[X,Y]= meshgrid(x,y);
```

The command lines plot the flux distribution into figure (1), where *'contour()'* creates a contour plot containing isolines of data only whereas *'contourf()'* filled the contour plot containing isolines of data.

```
figure(1);
      [ c, h ] = contour( (Y-101)*TargetSize./201, (X-
101)*TargetSize./201, data, 10);
      [ c, h ] = contourf( (Y-101)*TargetSize./201, (X-
101)*TargetSize./201, data, 10);
```
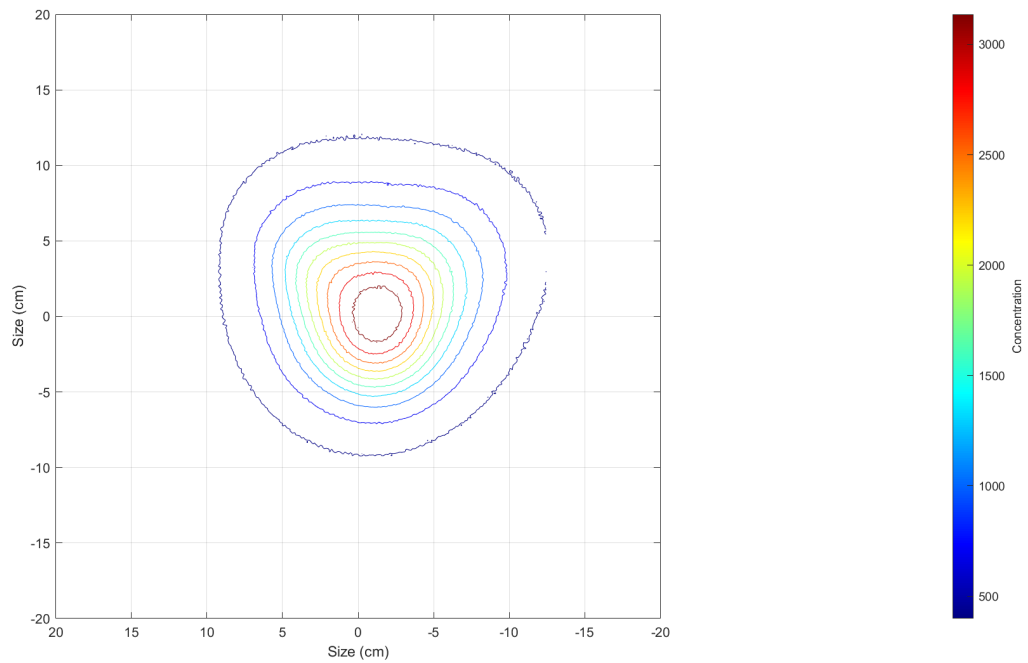
Figure 8 Example of simulated figure (1) from contour ()
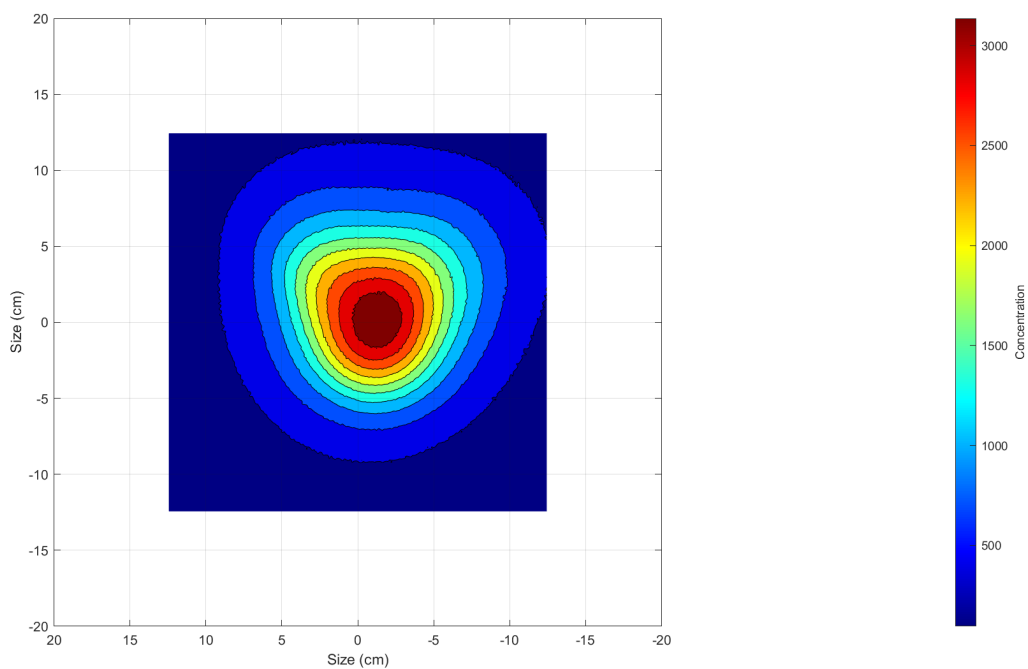
Figure 9 Example of simulated figure (1) from contourf()

While following command lines sets the appearance and behaviour of the figure.

```
grid on;
colormap(jet);
cb = colorbar;
caxis('auto');
LIMIT = 20;
axis( [-LIMIT LIMIT -LIMIT LIMIT] );
daspect( [1 1 1] );
shg;
%clabel(c,h);
%clabel(c,h,'manual');
view(270,90);
```

```
%Labeling Style
%v = 10:5e2:2e4; clabel( c, h, v, 'Fontsize', 8, 'Color', 'black',
'EdgeColor', 'black', 'BackgroundColor', 'c', 'LineStyle', '--',
'LineWidth', 0.1 );

  xlabel(cb,'Concentration');
  xlabel('Size (cm)');
  ylabel('Size (cm)');
```

The following command lines retain the figure 1 and calculates the total concentration in the square shape with increasing dimension of by integrating the concentration from 1cm x 1cm up to 25cm x 25cm. This code section is used to calculate the spillage.

```
hold on
  D=[]; E =[];
  min=0;
  for i=1:length(1:1:25)
  %min =10
  %min =3.5;
  min= min+0.5
  xv= [-min min min -min];
  yv= [-min -min min min];
  Xq= (Y-101)*TargetSize./201;
  Yq= (Y-101)*TargetSize./201;
  is_inside = inpolygon(Xq,Yq,xv,yv);
  integral = sum(data(is_inside));
  D(i)= integral;
  end
  E = transpose(D);
hold off
```

'Mesh' function creates a 3-D surface with respect to the concentration heights from the data is plotted to figure (2).

```
figure(2);
  mesh((Y-101)*TargetSize/201,(X-101)*TargetSize/201,data);
  %axis([-LIMIT LIMIT -LIMIT LIMIT])
    view(270,0)
```
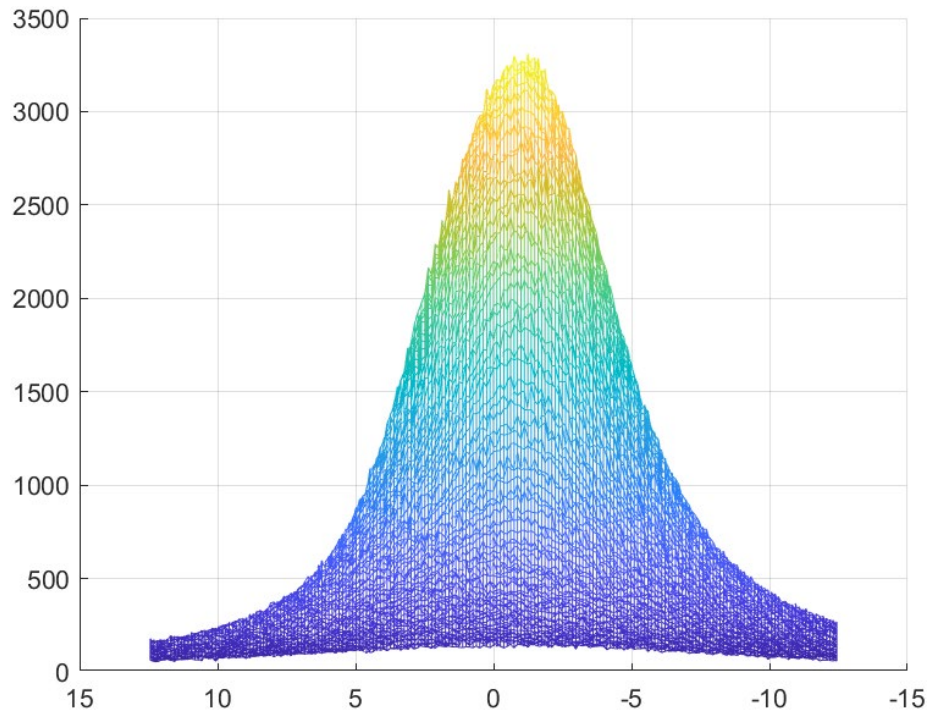
Figure 10 Example of simulated figure (2)

'*Plot()*' creates a 2-D line plot of the concentration in Y versus the corresponding values in X on figure(3).

```
figure(3);
  plot((Y-101)*TargetSize/201,data);
```
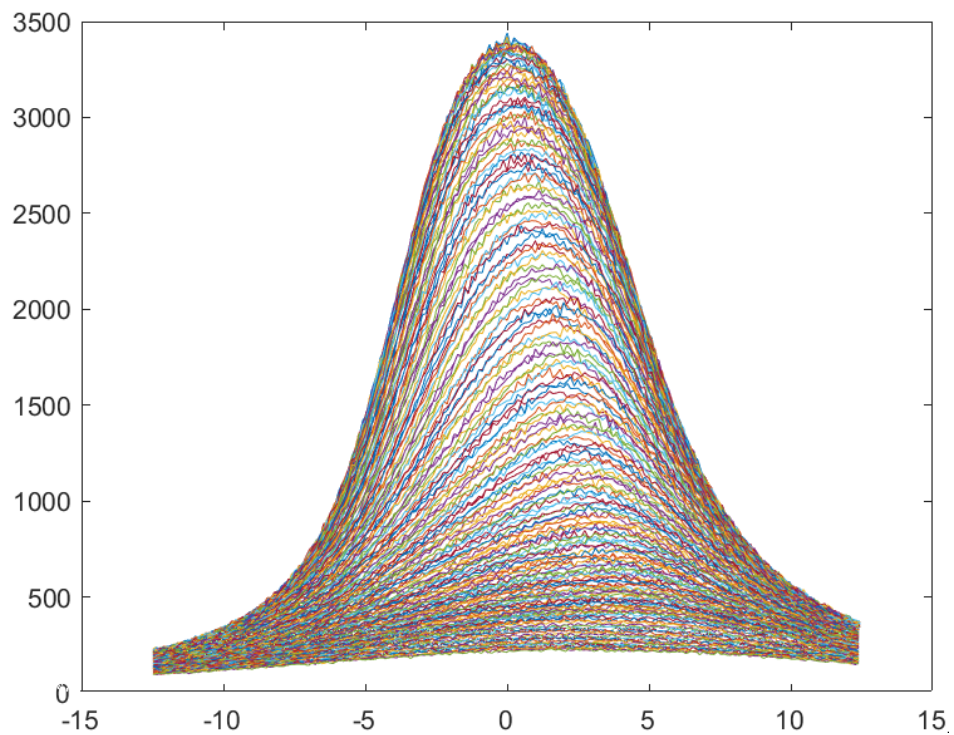

Figure 11 Example of figure (3)

4.2 Number of Ray and Corresponding Simulation Time

The number of rays is calculated as mentioned in section 3.4 for the simulation. It is to note that the simulator is CPU intensive, so the simulation time would also be improved with a better processor. Figure 12 shows that the simulation time is linearly proportional to the number of rays.

Table 7 Number of ray and Simulation time of corresponding mirror and solar disc resolutions

Nmr	Nsd	Nray	Simulation time (s)
47	20	354244640	8863
47	40	2798664800	35675
47	60	9352710480	71845
47	80	22093564480	140928
47	120	74280537120	305478
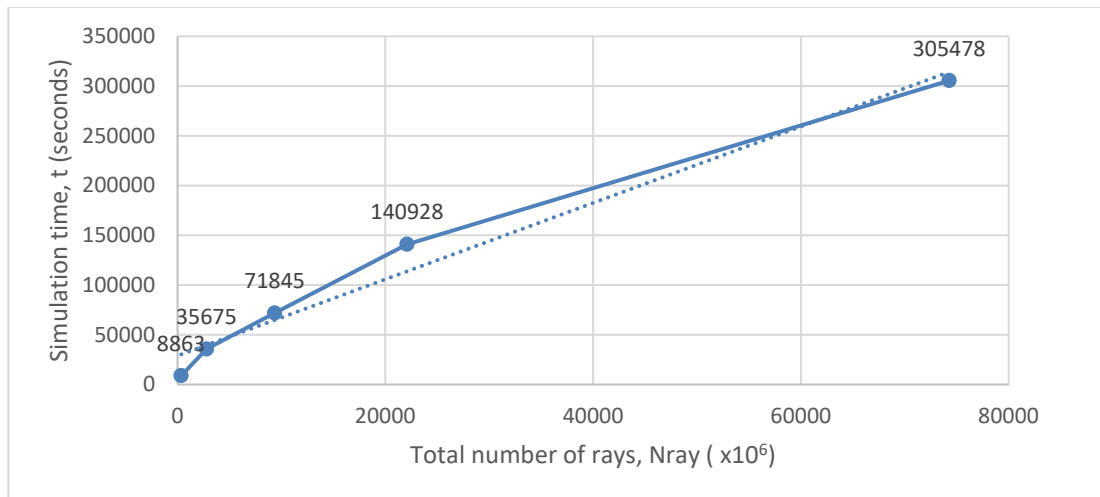
Figure 12 Number of ray and its corresponding simulation time

4.3 Comparison between Mirror Resolution and Solar Disc Resolution on Flux Distribution

The performance of the solar furnace system is simulated with increasing values of both n_{MR} and n_{SD} of 10, 30 and 60. The flux distribution profile is compared as shown in table 8 while table 9 and table 10 show the number of rays per disc for a fixed value of n_{SD} / n_{MR} with an increasing value of n_{MR} / n_{SD}.

From table 9 and 10, the ray/disc increases together with n_{SD}, while stayed constant for the fixed n_{SD} with the increasing of n_{MR}.

The comparison in table 8 shows that higher mirror resolution improve the shape of the flux profile most noticeably at the centre peak due to the number of ray per disc is constant throughout the increasing resolution of the solar disc. On the other hand, the number of rays per disc increases with a higher value of solar disc resolution resulting in lesser spikes and enhance the smoothness of the flux.

Table 8 Contour comparison of increasing n_{MR} and n_{SD}

	$n_{SD} = 10$	$n_{SD} = 30$	$n_{SD} = 60$
$n_{MR} = 10$			
$n_{MR} = 30$			
$n_{MR} = 60$			
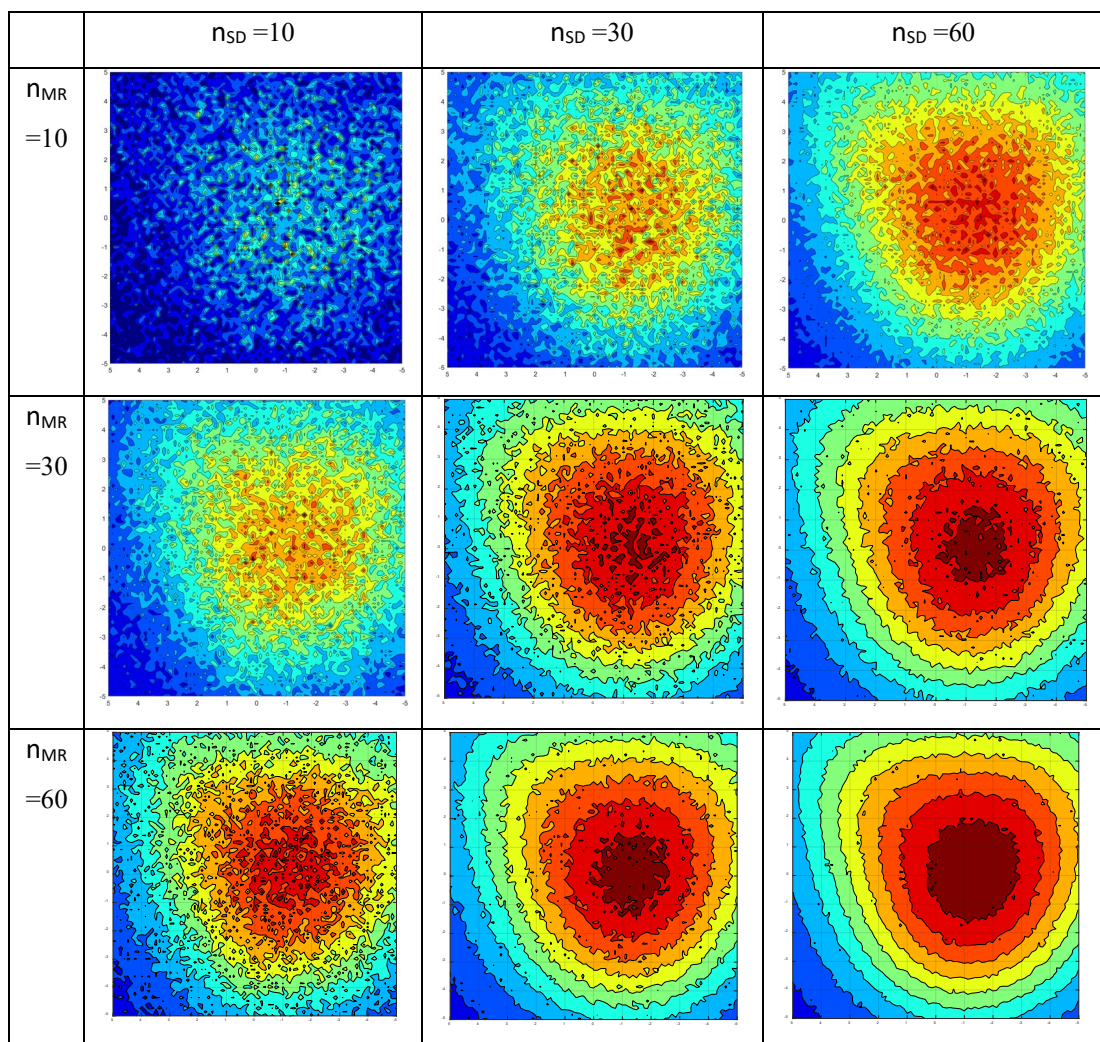
Table 9 Ray/ Disc for fixed n_{MR} with increasing n_{SD}

	$n_{SD} = 10$	$n_{SD} = 20$	$n_{SD} = 30$	$n_{SD} = 40$	$n_{SD} = 50$	$n_{SD} = 60$
$n_{MR} = 10$	332	1304	2912	5140	8000	11476
$n_{MR} = 60$	332	1304	2912	5140	8000	11476

Table 10 Ray/ Disc for fixed n_{SD} with increasing n_{MR}

	n_{MR} r= 10	$n_{MR} = 20$	$n_{MR} = 30$	$n_{MR} = 40$	$n_{MR} = 50$	$n_{MR} = 60$
$n_{SD} = 10$	332	332	332	332	332	332
$n_{SD} = 60$	11476	11476	11476	11476	11476	11476

4.4   Factors of k_1 and k_2 Resolution Effects

Table 8 shows the output mesh peak for the resolutions increased by the factors k1 and k2. As observed, the mesh peak has a high deviation at lower k1 and k2 factors. The profile is smoother and spikes are reduced as the resolution factor increases.

Table 11 Output peak of the NIFH for resolution in the function of k_1 and k_2

$k_1 = 5$				
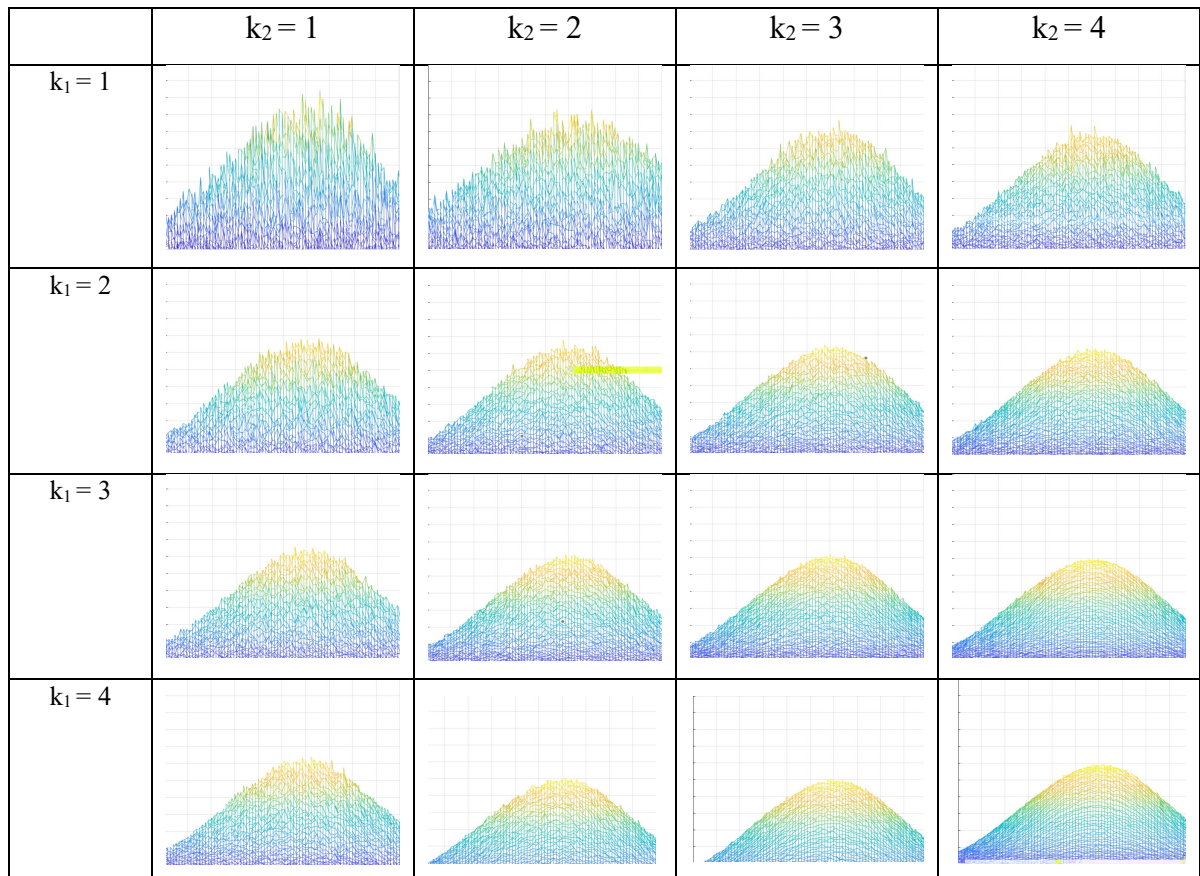
Figure 13 shows the maximum solar concentration ratio in the function of k_1 and k_2. The higher the k_1 and k_2 (high resolution) the smoother the flux distribution profile and the concentration become more constant and accurate. At low k_1 and k_2 (low resolution), the maximum solar concentration ratio is high because of the spikes and deviation throughout the flux profile. Table 12 shows the maximum solar concentration value, the concentration is around 3400 suns at a higher resolution. From the observation,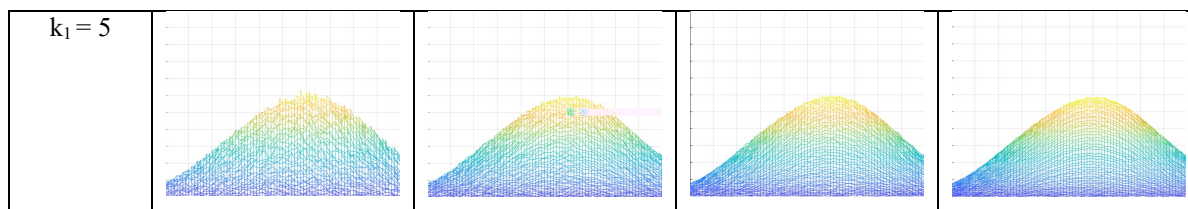 $k_1 = 4$ and $k_2 = 3$ already have a mature pattern which not much different from the mesh peak of the $k_1 = 5$, $k_2 = 4$. As shown in Figure 14, the simulation time taken in the function of k_1 and k_2 is increased quite significantly at higher resolution therefore, an optimal value of resolution with reasonably good results can be sufficient for the simulation work. High accuracy simulation result of solar flux distribution can be generated with a high number of mirror resolution and a high solar disc resolution. However, the simulation time will be increased by hours and days of simulation time. Therefore, highlighted cell in the table is recommended for the optimal resolution for accurate and mature patterns, with the shortest simulation time.
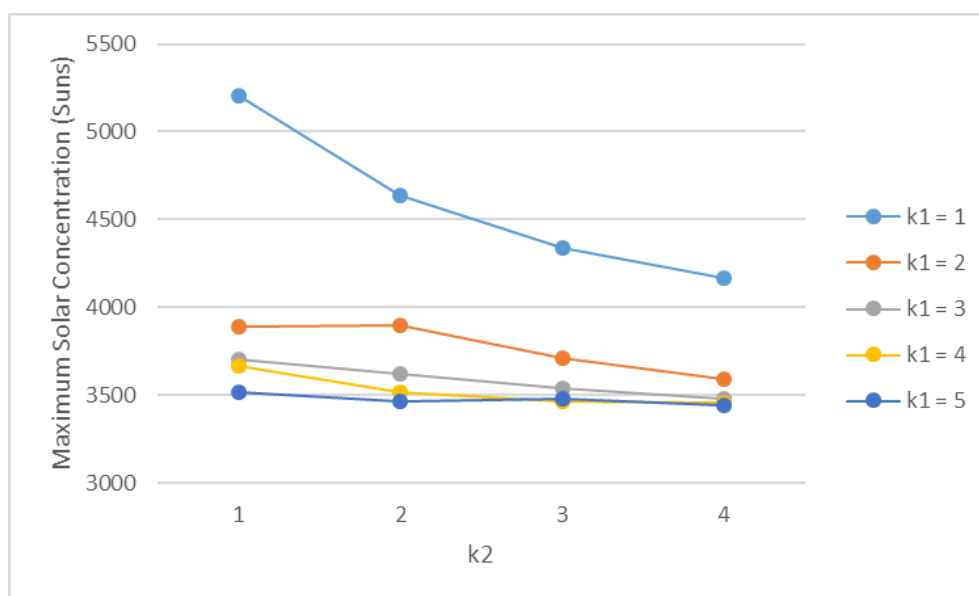
Figure 13 Maximum solar concentration ratio in the function of k_1 and k_2

Table 12 Maximum solar concentration in the function of k1 and k2

	$k_2 = 1$	$k_2 = 2$	$k_2 = 3$	$k_2 = 4$
$k_1 = 1$	5205	4639	4336	4165
$k_1 = 2$	3891	3896	3708	3594
$k_1 = 3$	3702	3619	3540	3476
$k_1 = 4$	3663	3515	3461	3455
$k_1 = 5$	3515	3464	3477	3443
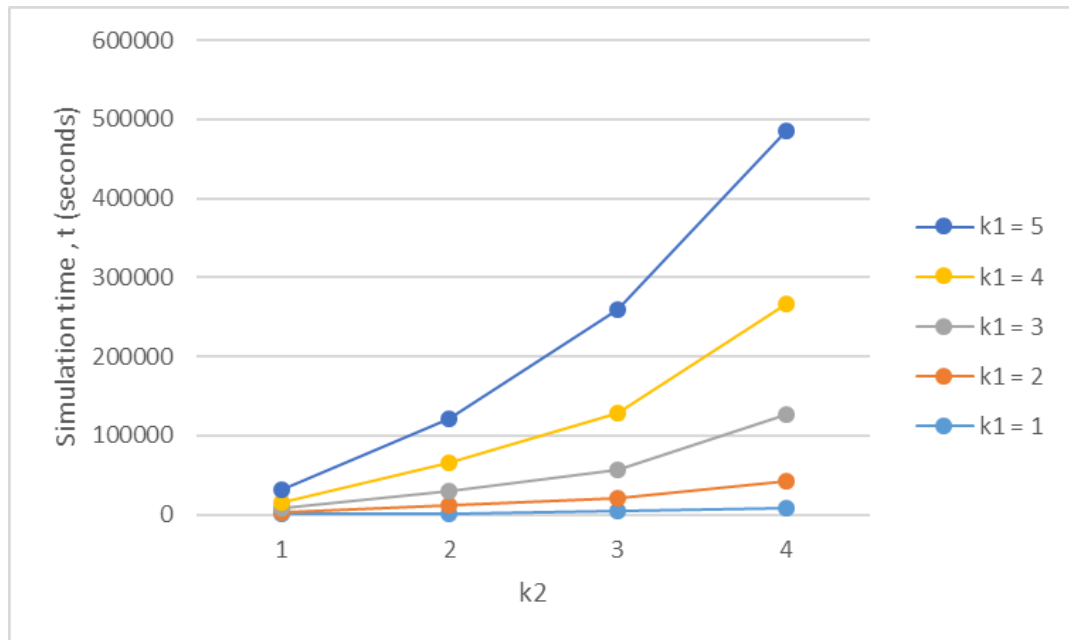
Figure 14 Simulation time in the function of k1 and k2

4.5 Slope Error and Circumsolar Ratio Effects on Spillage loss of NIFH

Figure 15, Figure 16, and Figure 17 show the spillage loss versus receiver size from 1cm to 25cm for CSR of 0.1, 0.2, and 0.3 at slope error of 1mrad, 2mrad, and 3mrad. From the simulation results, the spillage loss is quite severe for each CSR and SE. The Figure generated from the output is compared in table 13. As observed from the comparison table of flux profile between results without CSR SE and with CSR SE, the flux profile of CSR and SE are distorted and not fully in the receiver. This reduces the efficiency of the NIFH as the CSR and SE increase.

Figure 15 Spillage loss versus receiver size (square in shape) for CSR of 0.1, 0.2 and 0.3 in the case of SE = 1mrad

Figure 16 Spillage loss versus receiver size (square in shape) for CSR of 0.1, 0.2 and 0.3 in the case of SE = 2mrad
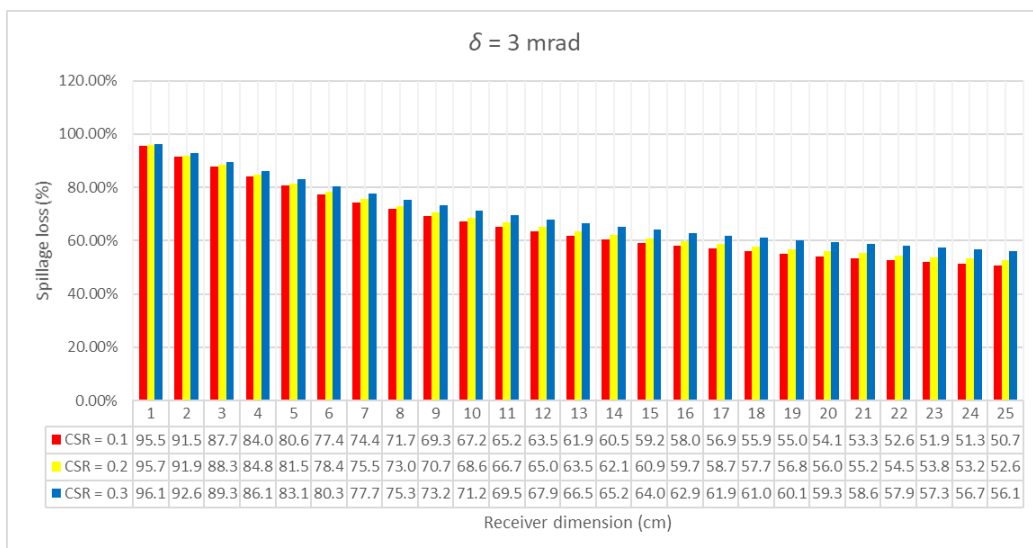
Figure 17 Spillage loss versus receiver size (square in shape) for CSR of 0.1, 0.2 and 0.3 in the case of SE = 3mrad

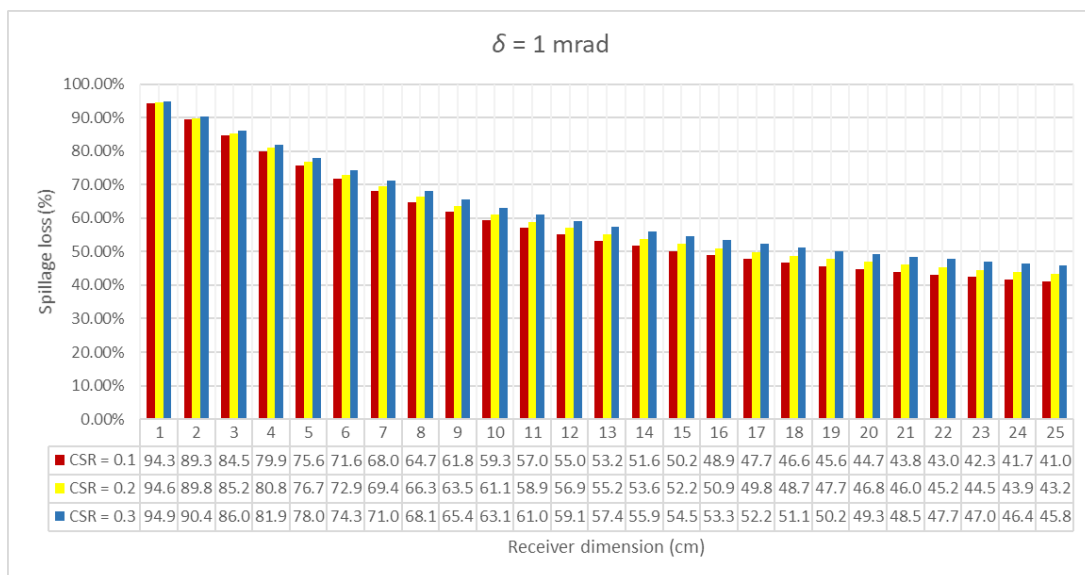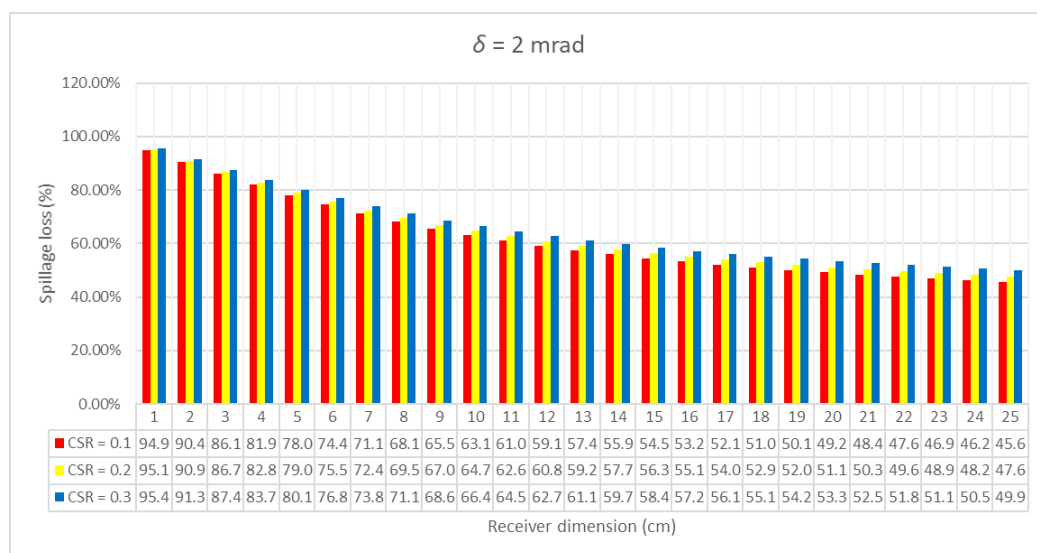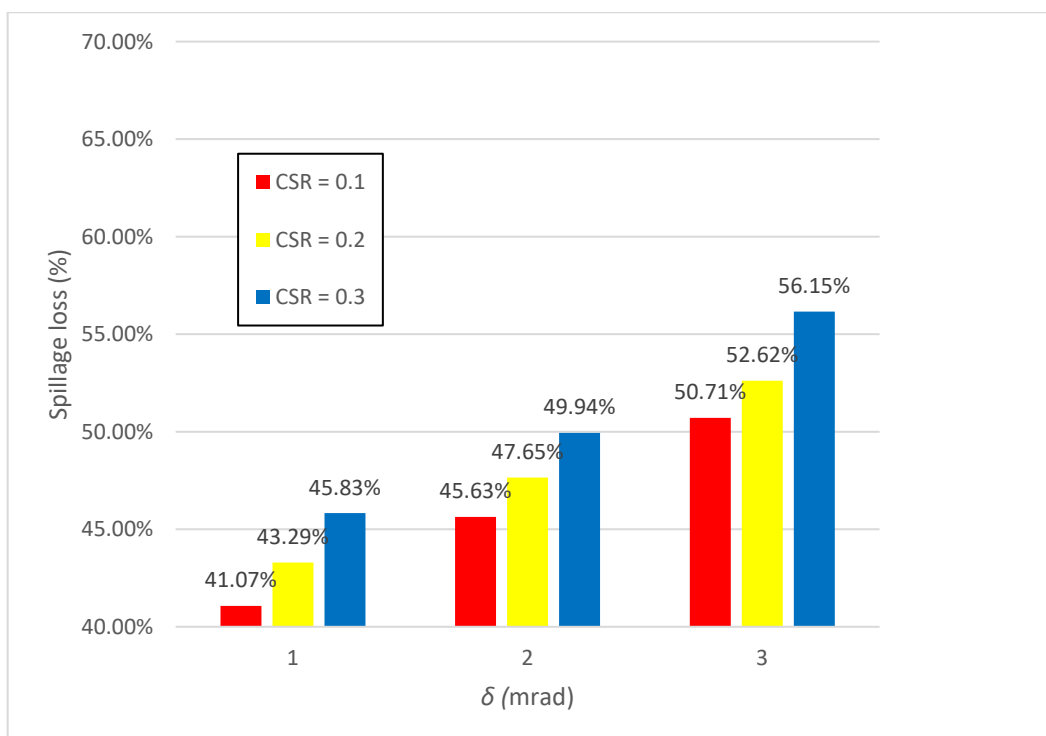Figure 18 Spillage loss of receiver for receiver dimension of 25cm x 25cm

Table 13 Output comparison

Without CSR and SE	With CSR and SE
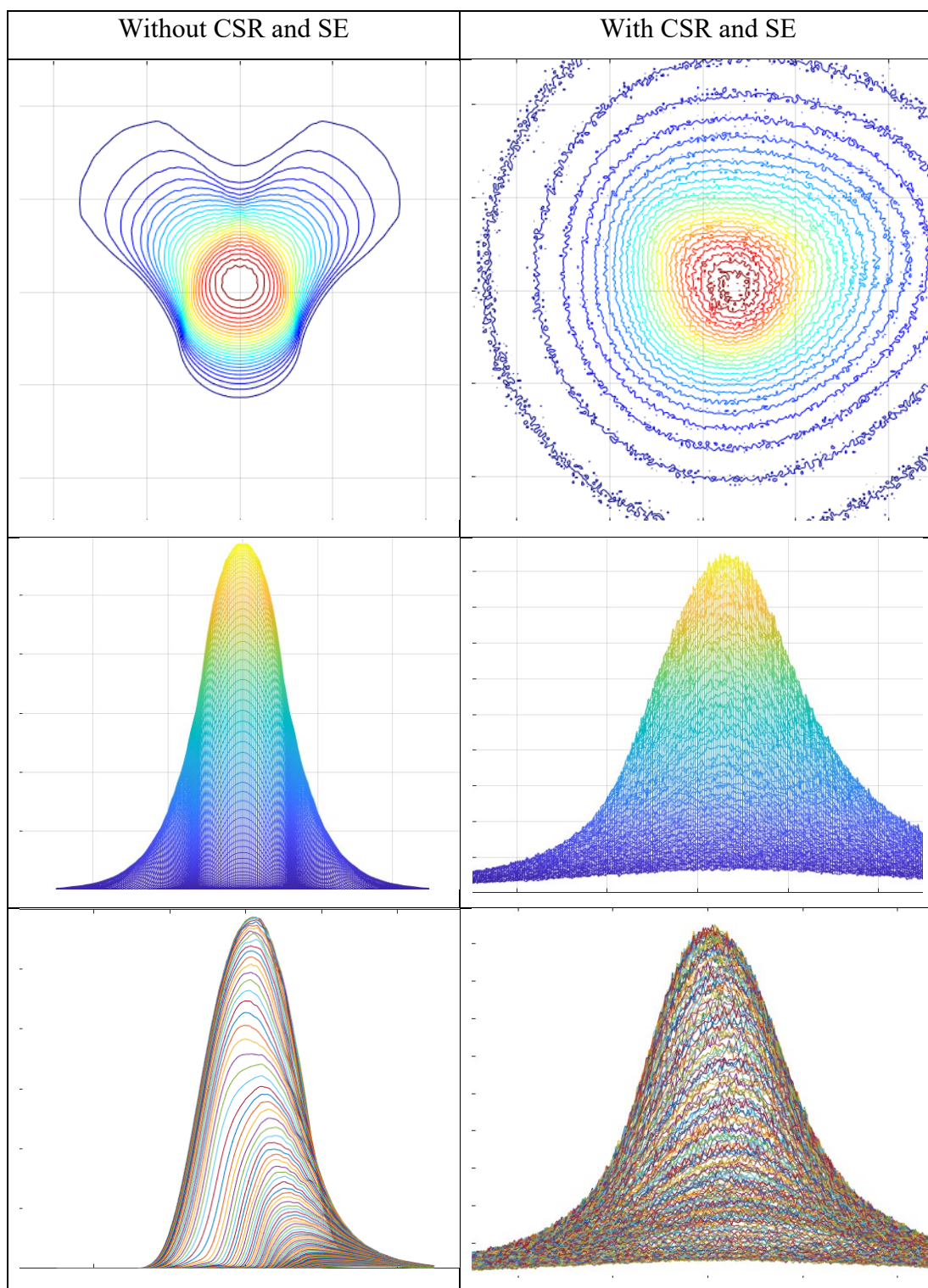
CHAPTER 5

CONCLUSIONS AND RECOMMENDATIONS

5.1   Conclusions

This work study the characteristics of the high-temperature solar furnace using NIFH with NIFH simulator and MATLAB. On the study of the relationship between the number of rays and the simulation time, the simulation time increased linearly with the number of rays. The number of rays determines the resolution of the output flux distribution, therefore higher ray number, higher simulation time with more accurate result. Therefore optimal resolution factor of k_1 factor to mirror resolution and k_2 factor to solar disc resolution is studied to obtain a reasonable and accurate result in the shortest time. In addition, the factor affecting the flux distribution profile for the heliostat such as circumsolar ratio and slope error is studied. The circumsolar ratio and slope error show to induces deterioration to the flux shape resulting in reduced heliostat performance with spillage loss as high as 40% for 25cm receiver size.

5.2   Recommendations for Future Work

The aspect that is not covered in the work and are interesting to investigate are:

1. Optimization for the pre-set parameters for lower astigmatism
2. Parameters such as Incident angle, target distance and offset distance effect on flux distribution profile.

REFERENCES

Chen, Y.T., Chong, K.K., Bligh, T. P., Chen, L.C., Yunus, J., Kannan, K.S., Lim, B.H., Lim, C. S., Alias, M. A., Bidin, N., Aliman, O., Salehan, S., S.A.H., Shk. Abd. Tam, Rezan, C. M., Tan, K. K., 2001. Non-imaging focusing heliostat. Solar Energy 71(3), 155-164.

Chen, Y.T., Chong, K.K., Lim, C.S., Lim, B.H., Tan, K.K., Aliman, O., Bligh, T.P., Tan, B.K., Ismail, G., 2002. Report of the first prototype of non-imaging focusing heliostat and its application in high temperature solar furnace. Solar Energy 72, 531–544.

Chen, Y.T., Chong, K.K., Lim, B.H., Lim, C. S., 2003. Study of Residual Aberration, Solar Energy Material and Solar Cell 79(1), 1-20.

Chen, Y.T., Kribus, A., Lim, B.H., Lim, C.S., Chong, K.K., Karni, J., Buck, R., Pfahl, A., Bligh, T.P., 2004. Comparison of two sun tracking methods in the application of heliostat field. Journal of Solar Energy Engineering 126(1), 638-644.

Chen, Y.T., Lim, B.H. and Lim, C.S., 2006. General sun tracking formula for heliostats with arbitrarily oriented axes.

Chen, Y.T., Chong, K.K., Lim, C. S., Lim, B.H., Tan, B.K., Lu, Y.F., 2006. Report on the second prototype of non-imaging focusing heliostat and its application in food technology. Solar Energy 79, 280-289.

Chen, Y.T., Lim, C.S., Ho, T.H., Lim, B.H., Wang, Y.N., 2009. Silicon Purification by a New Type of Solar Furnace. Chinese Physics Letter 26(7), 078103 (3 pages).
Chong, K.K., 2010a. Optimization of non-imaging focusing heliostat in dynamic correction of astigmatism for a wide range of incident angles. Optics Letters 35(10), 1614-6.

Chen Y.T., Ho T.H., Lim C.S., and Lim B.H., 2010. Development of silicon purification by strong radiation catalysis method, Chin. Phys. B Vol. 19, No. 11 (2010) 118105

Chong, K.K., 2010b. Optical analysis for simplified astigmatic correction of non-imaging focusing heliostat. Solar Energy 84, 1356-1365.

Chong, K.K., Tan, M.H., 2011a. Range of motion study for two different sun-tracking methods in the application of heliostat field. Solar Energy 85, 1837-1850.

Chong, K.K., Lim, C.Y., Hiew, C.W., 2011b. Cost effective solar furnace system using fixed geometry non-imaging focusing heliostat and secondary parabolic concentrator. Renewable Energy 36, 1595-1602.

Cressey,D.,2010.http://blogs.nature.com/news/2010/01/chinas_top_ten_science_achi
eve.html, Nature News Blog.

Lim, C.S., Li, L., 2009. Flux distribution of solar furnace using nonimaging focusing heliostat. Solar Energy 83, 1200–1210.

Lim, B.H., Chong, K.K., Lim, C.S. and Lai, A.C., 2016. Latitude-orientated mode of non-imaging focusing heliostat using spinning-elevation tracking method. Solar Energy, 135, pp.253-264.

Wang, Y., Potter, D., Asselineau, C.A., Corsi, C., Wagner, M., Caliot, C., Piaud, B., Blanco, M., Kim, J.S. and Pye, J., 2020. Verification of optical modelling of sunshape and surface slope error for concentrating solar power systems. Solar Energy, 195, pp.461-474.

Wong, C.W., Chong, K.K. and Tan, M.H., 2015. Performance optimization of dense-array concentrator photovoltaic system considering effects of circumsolar radiation and slope error. Optics express, 23(15), pp.A841-A857.

Zou, B., Yang, H., Yao, Y. and Jiang, Y., 2017. A detailed study on the effects of sunshape and incident angle on the optical performance of parabolic trough solar collectors. Applied Thermal Engineering, 126, pp.81-91.

APPENDICES

APPENDIX A: Tables

Table 14 Calculated spillage loss for SE =1mrad

SE = 1mrad	CSR		
Dimensions			
	0.1	0.2	0.3
1	94.34%	94.60%	94.90%
2	89.37%	89.87%	90.42%
3	84.56%	85.28%	86.08%
4	79.96%	80.89%	81.92%
5	75.63%	76.76%	78.01%
6	71.64%	72.94%	74.39%
7	68.02%	69.47%	71.08%
8	64.77%	66.35%	68.11%
9	61.88%	63.58%	65.46%
10	59.33%	61.11%	63.10%
11	57.07%	58.93%	61.01%
12	55.07%	56.99%	59.14%
13	53.28%	55.25%	57.46%
14	51.68%	53.69%	55.95%
15	50.23%	52.27%	54.58%
16	48.92%	50.99%	53.34%
17	47.72%	49.83%	52.21%
18	46.63%	48.76%	51.17%
19	45.64%	47.78%	50.22%
20	44.72%	46.88%	49.34%
21	43.88%	46.05%	48.53%
22	43.09%	45.28%	47.78%
23	42.37%	44.57%	47.08%
24	41.70%	43.91%	46.43%
25	41.07%	43.29%	45.83%

Table 15 Calculated spillage loss for SE =2mrad

SE = 2mrad	CSR		
Dimensions			
	0.1	0.2	0.3
1	94.92%	95.15%	95.40%
2	90.46%	90.90%	91.37%
3	86.13%	86.76%	87.46%
4	81.99%	82.80%	83.70%
5	78.08%	79.06%	80.15%
6	74.46%	75.59%	76.86%
7	71.16%	72.43%	73.84%
8	68.18%	69.57%	71.11%
9	65.52%	67.01%	68.66%
10	63.15%	64.72%	66.47%
11	61.03%	62.67%	64.51%
12	59.15%	60.85%	62.75%
13	57.46%	59.20%	61.17%
14	55.93%	57.72%	59.73%
15	54.55%	56.37%	58.43%
16	53.29%	55.15%	57.24%
17	52.14%	54.02%	56.15%
18	51.09%	52.99%	55.15%
19	50.12%	52.04%	54.23%
20	49.22%	51.17%	53.38%
21	48.40%	50.36%	52.59%
22	47.63%	49.61%	51.86%
23	46.92%	48.91%	51.18%
24	46.25%	48.26%	50.54%
25	45.63%	47.65%	49.94%

Table 16 Calculated spillage loss for SE =3mrad

SE = 3mrad	CSR		
Dimensions			
	0.1	0.2	0.3
1	95.51%	95.72%	96.10%
2	91.58%	91.96%	92.68%
3	87.76%	88.32%	89.35%
4	84.09%	84.82%	86.16%
5	80.63%	81.51%	83.13%
6	77.40%	78.42%	80.31%
7	74.45%	75.59%	77.71%
8	71.77%	73.02%	75.34%
9	69.36%	70.70%	73.20%
10	67.20%	68.62%	71.27%
11	65.26%	66.75%	69.53%
12	63.52%	65.07%	67.95%
13	61.94%	63.55%	66.53%
14	60.52%	62.17%	65.23%
15	59.22%	60.91%	64.04%
16	58.04%	59.76%	62.96%
17	56.95%	58.71%	61.96%
18	55.96%	57.73%	61.04%
19	55.03%	56.84%	60.18%
20	54.18%	56.00%	59.39%
21	53.38%	55.23%	58.65%
22	52.65%	54.51%	57.96%
23	51.96%	53.84%	57.32%
24	51.31%	53.21%	56.72%
25	50.71%	52.62%	56.15%

APPENDIX B: Developed Code

```matlab
clear
clc
clf

fid = fopen('C:\Directory Path\File Name.dat','r+');

[data,count]=fread(fid,[201,201],'double');

%data(1,1)= 0; % Abnormally high value error on simulator output at
(1,1)

x=1:201;
y=1:201;
global TargetSize %unit in cm
TargetSize=25;
[X,Y]= meshgrid(x,y);

Figure(1);
  %[ c, h ] = contour( (Y-101)*TargetSize./2001, (X-
101)*TargetSize./2001, data, 'levelstep',200);
  %[ c, h ] = contourf( (Y-101)*TargetSize./2001, (X-
101)*TargetSize./2001, data, 'levellistmode','auto');
    [ c, h ] = contour( (Y-101)*TargetSize./201, (X-
101)*TargetSize./201, data, 10);

  grid on;
  colormap(jet);
  cb = colorbar;
  caxis('auto');
  LIMIT = 20;
  axis( [-LIMIT LIMIT -LIMIT LIMIT] );
  daspect( [1 1 1] );
  shg;
  %clabel(c,h);
  %clabel(c,h,'manual');
  view(270,90);

%Labeling Style
  %h.LevelList = round(h.LevelList,0); % Set number of decimal
places to show in labels.
  %v = 10:1e2:2e4; clabel(c, h, v); % Selected contour lines to
label.
  %v = 10:2e2:6e3; clabel( c, h, v, 'Fontsize', 8, 'Color', 'black',
'EdgeColor', 'black' );
  %v = 10:5e2:2e4; clabel( c, h, v, 'Fontsize', 8, 'Color', 'black',
'EdgeColor', 'black', 'BackgroundColor', 'c', 'LineStyle', '--',
'LineWidth', 0.1 );

  xlabel(cb,'Concentration');
  xlabel('Size (cm)');
  ylabel('Size (cm)');
  %set(gca, 'XAxisLocation', 'origin', 'YAxisLocation', 'origin')

%Calculate the Total of the Concentration
  hold on
  D=[]; E =[];
  min=0;
```

```matlab
    for i=1:length(1:1:25)
    %min =10
    %min =3.5;
    min= min+0.5
    xv= [-min min min -min];
    yv= [-min -min min min];
    Xq= (Y-101)*TargetSize./201;
    Yq= (Y-101)*TargetSize./201;
    is_inside = inpolygon(Xq,Yq,xv,yv);
    integral = sum(data(is_inside));
    D(i)= integral;
    end
    E = transpose(D);
    hold off


figure(2);
    mesh((Y-101)*TargetSize/201,(X-101)*TargetSize/201,data);
    %axis([-LIMIT LIMIT -LIMIT LIMIT])
    view(270,0)

figure(3);
    plot((Y-101)*TargetSize/201,data);
    %ylim([0,5000]);
```